AIAA 2001–2845

Stability of Symmetric Vortices over Slender Conical Bodies at High Angles of Attack

Jinsheng Cai, Feng Liu
Department of Mechanical and Aerospace Engineering
University of California, Irvine, CA 92697-3975

Shijun Luo
Department of Aircraft Engineering
Northwestern Polytechnical University, Xi'an, China

31th AIAA Fluid Dynamics Conference and Exhibit
June 11–14, 2001/Anaheim, CA

Stability of Symmetric Vortices over Slender Conical Bodies at High Angles of Attack

Jinsheng Cai*, Feng Liu†
Department of Mechanical and Aerospace Engineering
University of California, Irvine, CA 92697-3975

Shijun Luo‡
Department of Aircraft Engineering
Northwestern Polytechnical University, Xi'an, China

Analyses are presented for the stability of a symmetric vortex pair over slender conical bodies in inviscid incompressible flow under small perturbations at high angles of attack. The bodies considered include circular cones and highly swept flat-plate wings with and without vertical fins, and elliptic cones of various eccentricities. The three-dimensional problem is reduced to a vortex stability problem for a pair of vortices in two-dimensions by using the conical flow assumption, classical slender-body theory, and postulated separation positions. The stability of vortices is then analyzed by a new method presented in a companion paper by the same authors. It is shown that the vortex asymmetry over a circular cone at high angles of attack is a result of the vortex instability under small anti-symmetric perturbations. There exists an intermediate cone with a finite thickness between the thick circular cone and the thin flat-plate delta wing, for which the symmetric vortices change from being unstable to being stable at a given angle of attack. The effects of the fin height and the separation position on the stability of the vortices are studied. Results agree well with known experimental observations.

I. Introduction

Separation vortices over highly-swept wings and slender bodies at high angles of attack are known to greatly increase the lift coefficient. However, the initially symmetric vortices may become asymmetric as the angle of attack is increased beyond a certain value, causing large rolling moments in the case of swept wings or large side forces in the case of slender bodies even at zero roll and yawing angles. The transition of the vortex pattern from being symmetric to asymmetric is of major importance for the performance and control of aircraft and other flight vehicles capable of extreme maneuvers. Much experimental, theoretical and computational work has been spent on the understanding, prediction, and control of the onset of vortex asymmetry (Ericsson and Reding[1] 1992). The basic physical mechanism of this transition, however, is not clear. At least two possible causes for the vortex asymmetry were suggested mainly based on experimental investigations: (1) inviscid hydrodynamic instability of the symmetrically separated vortices (Keener et al.[2] 1977); (2) asymmetric flow separation and/or asymmetric flow reattachment on each side of the body (Ericsson[3] 1992). There is at present no general agreement on the mechanism involved in the creation of the flow asymmetry.

Bird[4](1969) and Polhamus[5](1971) reported that the initially symmetric leading-edge vortices over slender delta wings became asymmetric at some high angle of attack before vortex breakdown occurred on the wing. However, Stahl et al.[6] (1992) revealed that no strongly asymmetric vortex flow was observed before vortex breakdown occurred on the wing in their water tunnel and wind tunnel experiments, and pointed out that the earlier observed onset of vortex asymmetry by Bird[4] (1969) was possibly related to different shapes in the leading edge of the delta wing models. The flat-plate wing model of Stahl et al.[6] (1992) has sharp edges, and the flat-plate wing model of Bird[4] (1969) has rounded leading edges. Stahl el al. conjectured that Bird's wing probably had near the apex the shape of a more or less thick elliptic cone rather than a thin flat-plate wing. However, Lim et al.[7] (2001) showed that the shape near the apex may not be wholly responsible for the vortex asymmetry by a water-tunnel test of flat plate wings of ogive-shaped planform with different tip and edge geometries, and that the edge geometry also played a crucial role. Ericsson[3] (1992) claims that the vortex asymmetry observed by Shanks[8] (1963) over slender flat-plate wings was likely caused by the asymmetric reattachment of the leading-edge separated flow on the leeside of the Shanks' models. There was a centerline spline mounted on the leeside of the flat-plate delta wing model of Shanks. Ericsson argued: "The reattaching flow can not find a stable

*Visiting Associate Researcher, Associate Professor, Northwestern Polytechnical University, Xi'an, China. Member AIAA.

†Associate Professor, Senior Member AIAA.

‡Distinguished University Professor.

stagnation point on the top of the centerline spline. As a result, the stagnation point move to one side of the centerline spline, forcing an asymmetry into the cross flow separation geometry, resulting in asymmetric leading-edge vortices."

It was found that the leeside vortex flow asymmetry over bodies of revolution could be suppressed by means of a fin between the vortices (Stahl[9] 1990 and Ng[10] 1990) or by flattening the nose into the elliptic cross section (Edwards 1978).[11]

Using numerical methods and the vortex line and vortex sheet models of inviscid and incompressible flow Dyer et al.[12] (1982) and Fiddes et al.[13] (1989) found asymmetric solutions as well as symmetric solutions for the vortex flow over slender conical bodies even though the separation lines were postulated symmetrically. These and many other numerical investigations suggested that the appearance of vortex asymmetry is an inviscid phenomenon (for example Lowson et al.[14] 1992, Fiddes[15] 1980).

Much work has been focused on experimental observation or numerical computation of the vortex motions behind slender bodies. There are only a few reports on the stability analysis of such systems. Using an inviscid incompressible model, Föppl[16] (1913) showed analytically that the vortex pair behind a circular cylinder can be stationary and is unstable under small anti-symmetric perturbations. Smith et al.[17] (1975) showed that a vortex pair behind a two-dimensional flat-plate can not be stationary. In the three-dimensional flow, Huang et al. (1996)[18] showed by an analytical method that the vortex pair over a slender flat plate delta wing can be stationary and is stable under small perturbations for angles of attack up to about two times the semi-apex angle of the wing.

The authors of this paper derived a new general stability condition for two-dimensional vortex flows in a companion paper (Cai et al.[19] 2001). This condition can be easily tested either analytically or numerically. We here extend the use of this newly developed stability condition to the study of three-dimensional symmetric vortices over slender conical bodies at high angles of attack. Following a summary of the two-dimensional vortex stability conditions, a conical flow theory is presented in this paper. The three-dimensional potential flow over slender conical bodies can be reduced to the solution of a two-dimensional problem in the conical coordinate system. This theory along with the two-dimensional vortex stability condition are subsequently applied to investigate the stability of the initially symmetric vortex flow over slender circular cones and highly swept flat-plate delta wings with and without vertical fins, and slender elliptic cones of various eccentricities.

II. Stability Condition for vortices in Two Dimensions

A general stability condition for the motion of a vortex or a group of vortices in a two-dimensional space is developed by the authors (Cai et al., 2001).[19] The results are summarized below.

Consider a system of vortices in two-dimensions. Assume one of the vortices in the system is located at (x, y). As this vortex is moved in the physical plane, other vortices in the system may move accordingly depending on the mode of motion under investigation, for instance, a symmetric or an anti-symmetric motion, and to satisfy boundary conditions. Assume the velocity for the vortex under consideration is a function of the vortex location (x, y), i.e.,

$$\begin{cases} u = u(x, y) \\ \\ v = v(x, y) \end{cases} \tag{1}$$

The stationary points (x_0, y_0) for the vortex satisfy

$$\begin{cases} u(x_0, y_0) = 0 \\ \\ v(x_0, y_0) = 0 \end{cases} \tag{2}$$

When the vortex is perturbed from its stationary point (x_0, y_0) and then let go, the vortex will follow the flow and may move back to its initial equilibrium position (stable), diverge from its initial equilibrium point (unstable), or move periodically around the equilibrium point (oscillating, neutrally stable) or stay at the initial perturbed position (non-oscillating, neutrally stable). Let J_0 be the Jacobian and D_0 the divergence of the vortex velocity field $\mathbf{q} = (u, v)$ at (x_0, y_0), where

$$J = \begin{vmatrix} \frac{\partial u}{\partial x} & \frac{\partial u}{\partial y} \\ \frac{\partial v}{\partial x} & \frac{\partial v}{\partial y} \end{vmatrix} \tag{3}$$

$$D = \nabla \cdot \mathbf{q} = \frac{\partial u}{\partial x} + \frac{\partial v}{\partial y} \tag{4}$$

The stability conditions by Cai et al. (2001)[19] for the vortex motion is summarized in Table 1.

	D_0	J_0	Comment
Stable	< 0	> 0	
Unstable	> 0	any	
	any	< 0	
Neutral	$= 0$	> 0	oscillating
	< 0	$= 0$	non-oscillating
	$= 0$	$= 0$	non-oscillating

Table 1 Stability Condition for Vortex Motion.

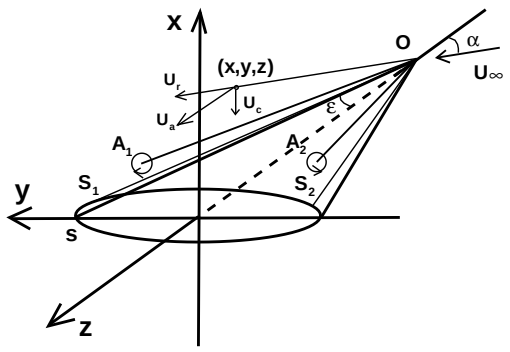

Fig. 1 Slender conical body and separation vortices.

III. Inviscid Conical Flow Model for Three-Dimensional Slender Bodies

Consider the flow past a slender conical body of an arbitrary symmetric cross section at an angle of attack α and zero sideslip as shown in Fig. 1. The plane of symmetry of the body Oxz coincides with the incidence plane of the flow. The body may have a slender triangular flat-plate fin on the top and/or the lower surface of the body in the plane of symmetry. The flow separates from the body surface along symmetric separation lines with respect to the symmetry plane of the body. Although separations are considered, the boundary layers that are responsible for the separations are ignored and the separation positions are postulated based on other methods, e.g., experimental data. The flow is assumed to be steady, inviscid incompressible, and conical.

Under the conical flow assumption, the separation lines OS_1 and OS_2 are assumed to be rays starting from the body apex O as shown in Fig. 1. In a real flow, a pair of vortex sheets erupt from the separation lines OS_1 and OS_2. They extend in the leeside of the body and then roll tightly into two concentrated vortices at a certain distance from the body. The distributed vortex sheets that connect the separation lines and the two concentrated vortices are neglected since their strength is in general much smaller than that of the two concentrated vortices. On the other hand, the two concentrated vortices can be approximated as a pair of vortex lines OA_1 and OA_2, which are also assumed to be rays from the body apex O under the conical flow assumption.

In an inviscid steady flow, a vortex line is a streamline. Based on experimental observations (e.g., Lim et al.[7] 2001), the two vortex lines stay relatively close to a slender body at high angles of attack. In addition, both pairs of the separation lines and the vortex lines are approximately conical rays coming off the body apex O. The body together with the separation vortices as a whole may then be considered slender and the flow may be assumed to be approximately conical in most part of the flow field except near the apex of the conical body or the base of the body of finite length, where neither the conical nor the slender body (small disturbance) assumption is valid.

Since the two tightly rolled vortices are fed by the vortex sheets coming off the separation lines on the body, the strength of the two concentrated vortices in our model must vary along the vortex lines directly in proportion to the distance from O. It must be noted that such an isolated vortex line with varying strength violates Helmholtz law on vortex strength. Nevertheless, it is admitted here as an approximation. In addition, there usually exists a secondary separation point between the primary separation point and the rear reattachment point in a practical flow. However, the secondary separation vortex is in general much weaker than the primary separation vortex. Therefore, the secondary vortex is ignored in the current model.

IV. Solution Method

The inviscid incompressible flow considered in the above model is potential except at the centers of the isolated vortices. The governing equation for the velocity potential is the three-dimensional Laplace equation with zero normal flow velocity on the body surface as the boundary condition. By the principle of superposition, the flow around the body can be obtained by solving the following two flow problems: (1) The flow due to the normal component of the freestream velocity; and (2) The flow due to the axial component of the freestream velocity, both subject to zero normal velocity at wall. We denote the velocity field of the first problem by $\mathbf{U}_1$ and that of the second problem by $\mathbf{U}_2$.

In the first problem, the slender body is placed normal to the cross flow component $U_n = U_\infty \sin\alpha$. Since the body is assumed to be slender, the velocity in the z direction due to three-dimensional effects can be neglected. The flow in each cross section at z may then be regarded as a two-dimensional flow across the local cross sectional profile governed by the two-dimensional Laplace equation with zero normal velocity at the wall. Solution to this two-dimensional velocity field can be obtained by conformal mapping or other analytical or numerical methods. For the simple profiles such as circles and ellipses with or without fins, $\mathbf{U}_1$ can be easily obtained by conformal mapping as was done in Cai et al.[19] (2001) and will be discussed in the following sections.

The second problem corresponds to the flow past a conical body with a freestream velocity $U_a = U_\infty \cos\alpha$ and zero angle of attack. As shown in Fig. 1, consider

the description of the same flow in two different but related coordinate systems. The first is the conventional orthogonal system (x, y, z). The second is the non-orthogonal conical coordinate system (x', y', r'). The two coordinate systems are related by the following affine transformation

$$(x', y', r') = (x/s, y/s, z) \tag{5}$$

where s is the semi-span of the body at z in the x-y plane, which is related to the semi-apex angle of the body ε by $s = z tan\varepsilon$. The unit vectors of the two coordinate systems are then related by the following equation

$$\begin{bmatrix} \mathbf{e}_x \\ \mathbf{e}_y \\ \mathbf{e}_z \end{bmatrix} = \begin{bmatrix} 1 & 0 & 0 \\ 0 & 1 & 0 \\ \frac{-x}{z} & \frac{-y}{z} & \frac{\sqrt{x^2+y^2+z^2}}{z} \end{bmatrix} \begin{bmatrix} \mathbf{e}_{x'} \\ \mathbf{e}_{y'} \\ \mathbf{e}_{r'} \end{bmatrix} \tag{6}$$

the velocity field $\mathbf{U}_2(x, y, z)$ can be described in the first coordinate system as

$$\mathbf{U}_2(x, y, z) = \mathbf{U}_p(x, y; z) + u_z(x, y, z)\mathbf{e}_z \tag{7}$$

where

$$\mathbf{U}_p(x, y; z) = u_x(x, y; z)\mathbf{e}_x + u_y(x, y; z)\mathbf{e}_y \tag{8}$$

The velocity potential for $\mathbf{U}_2(x, y, z)$ satisfies the three-dimensional Laplace equation, subject to the boundary condition of zero normal velocity at the body surface. Under the assumption of small perturbations for slender bodies, however, $u_z(x, y, z) = U_a$. Consequently, the three-dimensional problem can be simplified to a two-dimensional potential flow problem for the velocity vector $\mathbf{U}_p(x, y; z)$. The subscript p is used to indicate that the velocity field $\mathbf{U}_p$ is a potential flow and can be obtained by solving the two-dimensional Laplace equation in the x-y plane with z being a parameter for each cross section of the body.

The velocity field $\mathbf{U}_2$ depends only on $x' = x/s$ and $y' = y/s$ due to the conical flow assumption that the flow velocities are constant along rays from the body apex. Therefore, the velocity field $\mathbf{U}_2$ can be described in the non-orthogonal conical coordinate system (x', y', r') as

$$\mathbf{U}_2(x, y, z) = \mathbf{U}_{p'}(x', y') + u_{r'}(x', y')\mathbf{e}_{r'} \tag{9}$$

where

$$\mathbf{U}_{p'}(x', y') = u_{x'}(x', y')\mathbf{e}_{x'} + u_{y'}(x', y')\mathbf{e}_{y'} \tag{10}$$

With the help of Eqn. (6), Eqns (7), (8), (9) and (10) give

$$u_{r'}(x', y') = U_a\sqrt{x^2 + y^2 + z^2}/z \tag{11}$$

and the relation between $\mathbf{U}_{p'}(x', y')$ and $\mathbf{U}_p(x, y; z)$

$$\mathbf{U}_{p'}(x', y') = \mathbf{U}_p(x, y; z) + \mathbf{U}_c(x', y') \tag{12}$$

where

$$\mathbf{U}_c(x', y') = -\frac{U_n}{K}(x'\mathbf{e}_{x'} + y'\mathbf{e}_{y'}) \tag{13}$$

and K is the Sychev similarity parameter (Sychev,[20] 1960)

$$K = \tan\alpha/\tan\varepsilon \tag{14}$$

In the complex velocity form, $\mathbf{U}_c(x', y')$ becomes

$$u_c - iv_c = -\frac{U_n\overline{Z}}{Ks} \tag{15}$$

From equation (12), the three-dimensional boundary condition for $\mathbf{U}_2$ on the body surface can be expressed as

$$[\mathbf{U}_{p'}(x', y') + u_{r'}(x', y')\mathbf{e}_{r'}] \cdot \mathbf{n} = 0 \tag{16}$$

where $\mathbf{n} = \mathbf{n}_c + n_z\mathbf{e}_z$ is the normal vector to the three-dimensional body surface and $\mathbf{n}_c$ is the normal vector to the two-dimensional cross sectional profile of the body at a given z.

Notice that $\mathbf{U}_{p'}$ and $\mathbf{e}_z$ are orthogonal and also $\mathbf{e}_{r'} \cdot \mathbf{n} = 0$ on the surface of the conical body. We obtain the following two-dimensional wall boundary condition for $\mathbf{U}_p$

$$\mathbf{U}_p(x, y; z) \cdot \mathbf{n}_c = -\mathbf{U}_c(x', y') \cdot \mathbf{n}_c \tag{17}$$

The velocity $\mathbf{U}_c(x', y')$ represents the flow velocity drawn towards the body axis when the axial flow is decomposed into a velocity along the conical ray and the velocity in the cross sectional plane. At the surface of the body, the normal component of this velocity must be canceled by the potential field $\mathbf{U}_p$. Physically, $\mathbf{U}_p$ represents the displacement effect of a non-zero thickness body.

$\mathbf{U}_{p'}$ is not a potential flow field but it can be obtained by solving the potential field $\mathbf{U}_p$ in the two-dimensional plane (x, y) subject to the boundary condition given by Eqn. (17). In the case of a circular cone, the solution is simply one single point source, which can be written in the complex velocity format as

$$u_p - iv_p = \frac{U_n s}{KZ} \tag{18}$$

where $s = a$ is the radius of the cone at z. In the case of the triangular flat-plate wing, the solution becomes

$$u_p - iv_p = 0 \tag{19}$$

since the right-hand-side of Eqn. (17) is zero for a zero thickness flat-plate wing.

For more complex geometries, $\mathbf{U}_p$ can be obtained by a singularity method, e.g., by distributing point sources within the body contour. The complex velocity at the point $Z = x + iy$ due to N point sources at $Z_j = x_j + iy_j$ can be written as

$$u_p - iv_p = \frac{1}{2\pi}\sum_{j=1}^{N}\frac{Q_j}{Z - Z_j} \tag{20}$$

where Q_j is the strength of the point sources and $Q_j (j = 1, 2, ...N)$ are to be determined by N simultaneous equations of the boundary condition on the body contour.

Notice that $\mathbf{U}_1$ and $\mathbf{U}_p(x, y; z)$ depend only on x' and y'. On superposition, the complete three-dimensional flow field is represented in the non-orthogonal conical coordinate system as

$$\mathbf{U}(x', y') = \mathbf{V}(x', y') + u_{r'}(x', y')\mathbf{e}_{r'} \qquad (21)$$

where

$$\mathbf{V}(x', y') = \mathbf{U}_1(x', y') + \mathbf{U}_p(x', y') + \mathbf{U}_c(x', y') \quad (22)$$

Notice that $\mathbf{V}(x', y')$ is a two-dimensional velocity vector field in the plane ($\mathbf{e}_{x'}$, $\mathbf{e}_{y'}$) and the $u_{r'}(x', y')\mathbf{e}_{r'}$ term in Eqn. (21) is a velocity component in the ray direction $\mathbf{e}_{r'}$ which does not contribute to the flow velocity in the plane ($\mathbf{e}_{x'}$, $\mathbf{e}_{y'}$). Consequently, the stability of the flow system can be analyzed by studying only the two-dimensional 'flow field' in Eqn. (22) $\mathbf{V}(x', y')$. The vortex stability condition by Cai, et al[19] (2001) as summarized in Table 1 will then readily apply.

V. Conditions on Vortex Location, Separation, and Reattachment

For an inviscid flow, a stationary vortex line must be a streamline. In the current conical model, the vortex lines are assumed to be rays coming off the body apex. Therefore, the flow velocity $\mathbf{V}(x', y')$ in the cross sectional plane must be zero at the center of each vortex. This provides the condition for stationary vortex positions. Notice, however, the induced velocity on a vortex line due to the vortex itself is zero. This is justified by replacing the vortex line by the Rankine vortex filament (for example Saffman[21] 1992). At the center of the vortex filament, the induced velocity by the vortex itself is zero.

The separation and reattachment lines are also assumed to be conical rays on the body surface from the body apex. The flow velocity must be tangential to these lines. The velocity on either side of a separation line must move towards the line, whereas the velocity near a reattachment line must move away from the line. This corresponds to the condition that the velocity $\mathbf{V}(x', y')$ must be zero for both separation and reattachment points and must move towards a separation point and move away from a reattachment point.

VI. Analyses of Typical Slender Conical Bodies

The above flow model and stability theory are used in this Section to analyze the stability of symmetric vortices over a number of typical slender conical bodies. Comparisons with experimental data are made whenever available.

A. Slender Circular Cones

A circular cone of semi-apex angle ε at an angle of attack α and no sideslip is considered. Fig. 2 shows the circular cross section of the body at a given distance from the apex, where a is the radius of the circular cross section, h_W and h_L are the heights of the windward and leeward splitter plates that may be added to the cone. The separation lines are postulated to be symmetric with respect to the incidence plane Oxz. The position of the separation line OS_1 is specified by the angle θ_0 in the x-y plane measured in the anticlockwise direction starting from the leeward side end of the cone. In the cross flow plane, the initially stationary symmetric vortices of strength Γ are located at $Z_0 = x_0 + iy_0$ and $\overline{Z_0} = x_0 - iy_0$. By the method presented in the proceeding sections, the velocity at any point $Z = x + iy$ except the vortex points Z_0 and $\overline{Z_0}$ is given in the complex velocity form

$$\begin{aligned} u - iv &= U_n(1 - a^2/Z^2) + \frac{i\Gamma}{2\pi}\left(\frac{1}{Z - Z_0}\right. \\ &- \left.\frac{1}{Z - \overline{Z_0}} - \frac{1}{Z - a^2/\overline{Z_0}} + \frac{1}{Z - a^2/Z_0}\right) \\ &- \frac{U_n\overline{Z}}{aK} + \frac{U_n a}{KZ} \end{aligned} \qquad (23)$$

On the right hand side of the above equation, the first two terms are the $\mathbf{U}_1$ term due to the normal velocity component of the freestream flow U_n, and the last two terms are due to the axial velocity component of the freestream flow U_a, namely Eqns. (15) and (18). The tangential velocity on the body contour is obtained by substituting $Z = ae^{i\theta}$ in Eqn. (23). The velocity at the vortex point Z_0 is obtained by removing the induced velocity term due to the vortex at Z_0 itself, i.e.,

$$\begin{aligned} u_0 - iv_0 &= U_n(1 - a^2/Z_0^2) + \frac{i\Gamma}{2\pi}\left(-\frac{1}{Z_0 - \overline{Z_0}}\right. \\ &- \left.\frac{1}{Z_0 - a^2/\overline{Z_0}} + \frac{1}{Z_0 - a^2/Z_0}\right) \\ &- \frac{U_n\overline{Z_0}}{aK} + \frac{U_n a}{KZ_0} \end{aligned} \qquad (24)$$

The stationary symmetric vortex position Z_0 and the vortex strength Γ are determined by solving the following three simultaneous equations for x_0, y_0, and Γ. Two equations are from Eq. (24), by requiring $u_0 - iv_0 = 0$. Another condition requires that the flow velocity given by Eqn. 23 be zero at a separation point $Z = ae^{i\theta_0}$ to determine the separation location θ_0 on the wall. The velocities on both sides of $\theta = \theta_0$ must be towards the point $\theta = \theta_0$.

As an example, consider the case of a circular cone with semi-angle $\varepsilon = 8^\circ$ at an angle of attack $\alpha = 38^\circ$, corresponding to $K = 5.5591$. Fig. 2 shows a cross section of the body. The solid lines off the circular body

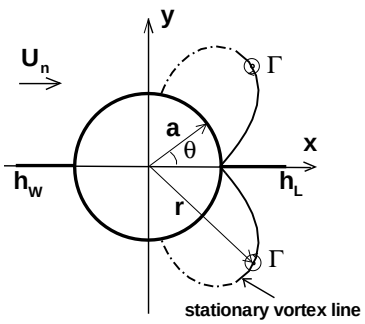

Fig. 2 Stationary vortex line for a circular cone with or without fin, $K = 5.5591$.

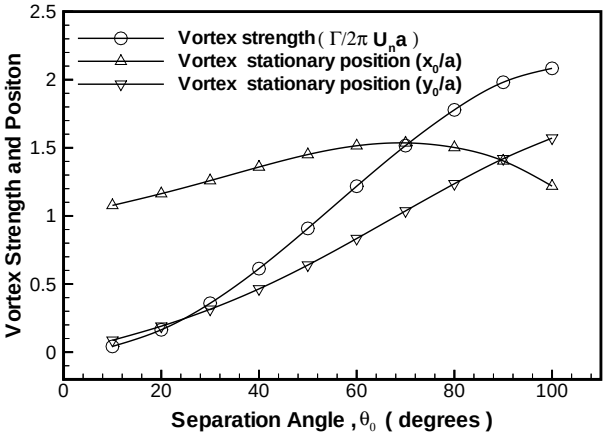

Fig. 3 Stationary vortex position and vortex strength vs. separation angle for a circular cone, $K = 5.5591$.

are locations where the two symmetric vortices can be stationary while resulting in a flow field with separation points on the body surface. The strength and position of the vortices vs. the separation angle are plotted in Fig. 3. As the vortices move away from the rear stagnation point along the stationary path, the vortex strength increases monotonically and the separation angle increases from 0° to about 100°. Further movement along the path results in a flow field that has no separation point on the surface of the circular body. This is marked by the dashed lines in Fig. 2.

The stationary symmetric vortex positions obtained by the present analytical method for different values of the similarity parameter K at the separation angle $\theta_0 = 34°$ are compared in Fig. 4 with the numerical solutions given by Dyer et al. (1982),[12] who used Bryson's vortex line model for the slender circular cone in an incompressible inviscid flow. The results agree well at large K values. The differences at lower K values may be attributed to the differences in the models

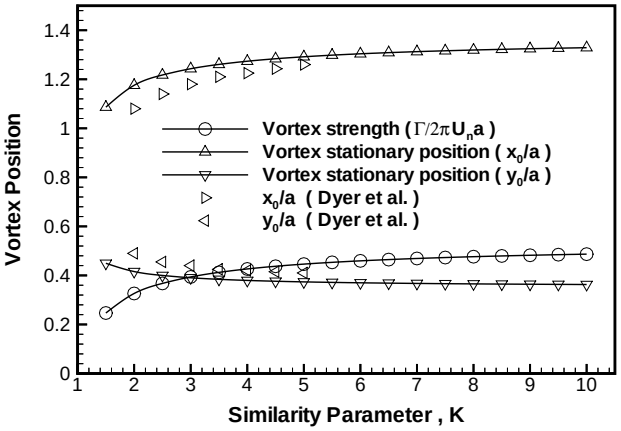

Fig. 4 Stationary symmetric vortex position for a circular cone, comparison with Dyer et al. (1982),[12] $\theta_0 = 34°$.

used by the two methods. Fig. 4 also shows the vortex strength vs. K for this case.

To study their stability, the symmetric vortices are slightly perturbed from their stationary positions, i.e., from Z_0 and $\overline{Z_0}$ to Z_1 and Z_2, respectively. Only positions on the solid part of the stationary lines in Fig. 2 are considered since the solutions with the vortices on the dashed lines are non-physical. The strength of the vortices is kept constant because the perturbations are small and instant. The complex velocity at the vortex located at Z_1 is found by removing the induced velocity term due to the vortex at Z_1 itself.

$$\begin{aligned} u - iv &= U_n(1 - a^2/Z_1^2) + \frac{i\Gamma}{2\pi}\left(-\frac{1}{Z_1 - Z_2}\right. \\ &- \left.\frac{1}{Z_1 - a^2/\overline{Z_1}} + \frac{1}{Z_1 - a^2/\overline{Z_2}}\right) \\ &- \frac{U_n\overline{Z_1}}{aK} + \frac{U_n a}{KZ_1} \end{aligned} \tag{25}$$

The stability conditions outlined in the previous section are then applied to the above equation in terms of Z_1. The perturbation is decomposed into a symmetric perturbation and an anti-symmetric perturbation. For a symmetric perturbation,

$$Z_1 = Z_0 + \Delta Z, \qquad Z_2 = \overline{Z_0} + \overline{\Delta Z} \tag{26}$$

For an anti-symmetric perturbation,

$$Z_1 = Z_0 + \Delta Z, \qquad Z_2 = \overline{Z_0} - \overline{\Delta Z} \tag{27}$$

where $\Delta Z = \Delta x + i\Delta y$ is the perturbation, and $|\Delta x| \ll a$, $|\Delta y| \ll a$. After inserting Eqns. (26) and (27) into Eqn. (25), we can then easily calculate the divergence and Jacobian of the vortex velocity field (u, v) either analytically or numerically.

It is shown by Cai et al.[19] (2001) that D_0 is zero in the pure two-dimensional case. Thus, symmetric

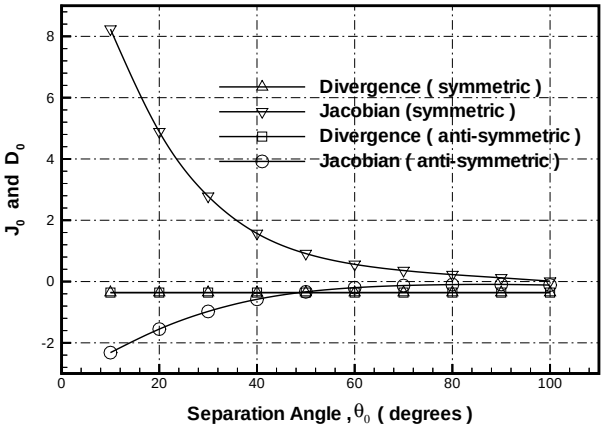

Fig. 5 Divergince and Jacobian vs. separation angle for a circular cone, $K = 5.5591$.

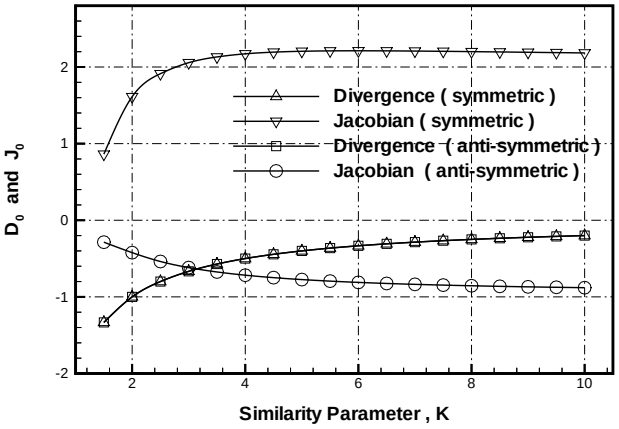

Fig. 6 Divergence and Jacobian vs. similarity parameter for a circular cone, $\theta_0 = 34^\circ$.

vortices behind a cylinder of any shape can only be neutrally stable ($J_0 \geq 0$) or unstable ($J_0 < 0$). Fig. 5 shows the dimensionless divergence D_0 and the dimensionless Jacobian J_0 at (x_0, y_0) versus the separation angle θ_0 for the three-dimensional circular cone case when $K = 5.5591$. For simplicity, D_0 and J_0 in Fig. 5 and all other figures denote the dimensionless values $D_0 L/U_n$ and $J_0 L^2/U_n^2$, respectively, where L is a length scale. In this case $L = a$. It is seen that D_0 is a non-zero constant for both the symmetric and anti-symmetric perturbations. In fact, D_0 is produced by $\mathbf{U}_c$ in Eqn. (13) or (15), which is induced by the axial component U_a of the incoming flow and is valid for all the slender conical bodies. The other terms of the vortex velocity expression of Eq. (25) have no contribution to D_0.

$$D_0 = -\frac{2U_n}{aK} \tag{28}$$

Therefore, for the slender conical body, the initially symmetric vortices are stable, neutrally stable or unstable, when the Jacobian, $J_0 > 0$, $J_0 = 0$, or $J_0 < 0$, respectively, according to the stability conditions listed in Table 1.

Fig. 5 shows that the Jacobian J_0 for symmetric perturbations is always greater than zero and the Jacobian J_0 for anti-symmetric perturbations is always less than zero for $K = 5.5591$, indicating that the symmetric vortices over the circular cone are stable under symmetric perturbations and unstable under anti-symmetric perturbations. Thus, the initially symmetric vortex flow over the slender circular cone tends to become asymmetric. This agrees with the well known experimental results, e.g., Asghar et al.[22] (1994).

The dependence of the vortex stability on the similarity parameter K for a fixed separation position $\theta_0 = 34^\circ$ is shown in Fig. 6. It is seen that the vortex instability increases monotonically as K increases. For a circular cone of a given apex angle, this means that the asymmetry tendency for the initially symmetric vortex pair increases as the angle of attack α increases. It is known from experimental data that the vortices become asymmetric for the circular cone when K is approximately 2 (for example, Keener et al.[2] 1977). This is not well predicted by the present simplified model, as Fig. 6 shows that the symmetric vortices are unstable under anti-symmetric perturbations when K is as low as 1.5 with the postulated separation point $\theta_0 = 34^\circ$.

Figs. 3 and 4 show that the vortex coordinates x and y remain close to the conical body. This indicates that the slenderness assumption of the body-vortex combination is a good assumption even for large values of K and the separation angle. This is true for all other cases studied in this paper.

B. Slender Circular Cones with Fins

The two-dimensional stability analyses by Cai et al.[19] (2001) show that adding a flat-plate fin of sufficient length to the rear end of a circular cylinder stabilizes the symmetric vortices behind the circular cylinder under anti-symmetric perturbations.

In three dimensions this is equivalent to adding a triangular flat-plate fin on the leeside of the circular cone in the symmetry plane. In general, a windward side fin of this type may also be added. A cross section of a circular cone with both the leeward and windward fins corresponds to a two-dimensional circular cylinder of radius a with a leading fin and a trailing fin as shown in Fig. 2. The two fins are characterized by the heights h_W and h_L measured from the center of the cylinder. The radius of the circle and the height of the fins must scale linearly with the distance z of the cross section from the nose of the circular cone. Thus, the ratios h_W/a and h_L/a determine the relative size of the fins to the circular cone.

The two-dimensional stability analysis in Cai et al.[19]

(2001) then suggests that adding a fin of sufficient size in the leeside may stabilize the vortices over a three-dimensional circular cone discussed in the previous section. Indeed, Asghar et al.[22] (1994) performed wind tunnel experiments of a circular cone of the semi-apex angle $\varepsilon = 8^\circ$ with and without a fin at an angle of attack $\alpha = 35^\circ$ ($K = 4.9822$). Measured circumferential pressure distribution and the ratio of side forces to normal forces along the cylinder indicate the flow behind the cone is asymmetric without a fin. When a leeward side fin of the size $h_L/a = 2$ is added to the circular cone, the flow becomes symmetric. Three-dimensional analysis of this problem is performed.

Since the fin is located in the symmetry plane of the body, it has no effect on the symmetric flows. The stationary symmetric vortex position and strength as function of θ_0 are the same as those of the circular cone without the fin (see Fig. 3).

By using the results of Section 5 of Cai et al. (2001)[19] and following the procedures of the above section, the complex velocity at the vortex point Z_1 is obtained by a limiting process (see Rossow[23] 1978).

$$\begin{aligned} u - iv &= \left[U_n(1 - a_1^2/\zeta_1^2) + \frac{i\Gamma}{2\pi}\left(-\frac{1}{\zeta_1 - \zeta_2}\right.\right. \\ &- \left.\left.\frac{1}{\zeta_1 - a_1^2/\overline{\zeta_1}} + \frac{1}{\zeta_1 - a_1^2/\overline{\zeta_2}}\right)\right]\left(\frac{d\zeta}{dZ}\right)_1 \\ &- \frac{i\Gamma}{4\pi}\left(\frac{d^2Z}{d\zeta^2}\right)_1\left(\frac{d\zeta}{dZ}\right)_1^2 \\ &- \frac{U_n\overline{Z_1}}{aK} + \frac{U_n a}{KZ_1} \end{aligned} \tag{29}$$

where the subscript 1 denotes the values at $Z = Z_1$ or $\zeta = \zeta_1$. The conformal mappings are

$$\zeta' = \frac{1}{2}\left(Z + \frac{a^2}{Z}\right) \tag{30}$$

$$\zeta' - X_m = \frac{1}{2}\left(\zeta + \frac{a_1^2}{\zeta}\right) \tag{31}$$

where

$$X_m = \frac{(a^2 + h_L^2)}{4h_L} - \frac{(a^2 + h_W^2)}{4h_W} \tag{32}$$

$$a_1 = \frac{(a^2 + h_L^2)}{4h_L} + \frac{(a^2 + h_W^2)}{4h_W} \tag{33}$$

and from Eqs. (30) and (31)

$$\frac{d\zeta}{dZ} = \frac{\zeta^2(Z^2 - a^2)}{Z^2(\zeta^2 - a_1^2)} \tag{34}$$

$$\frac{d^2Z}{d\zeta^2} = \frac{2}{(Z^2 - a^2)\zeta^3}\left[a_1^2Z^2 - \frac{a^2Z^3(\zeta^2 - a_1^2)^2}{(Z^2 - a^2)^2\zeta}\right] \tag{35}$$

It is noted that when the two vortex points are not symmetric with respect to the real axis, vortices will be shed from the sharp edges of the fins to satisfy

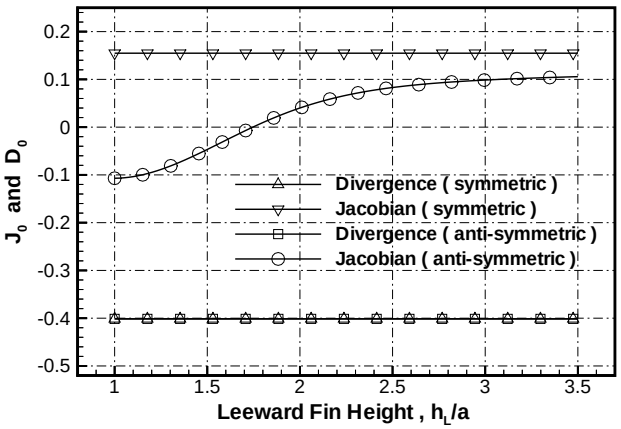

Fig. 7 Divergence and Jacobian vs. leeward fin height for a circular cone, $K = 4.9822, \theta_0 = 85^\circ$**,** $h_W = 0.0$**.**

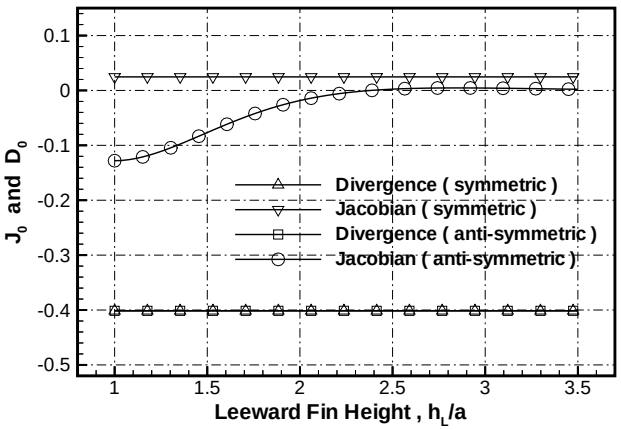

Fig. 8 Divergence and Jacobian vs. leeward fin height for a circular cone, $K = 4.9822, \theta_0 = 95^\circ$**,** $h_W = 0.0$**.**

Kutta condition. Under the small perturbation assumption, however, the strength of such vortices is much weaker than that of the original symmetric vortex pair. Therefore, the shed vortex is ignored in Eq. 29 for the anti-symmetric perturbation investigation. The transformed values ζ_1 and ζ_2 of Z_1 and Z_2 can be obtained by Eqns. (30) and (31). The symmetry properties preserve under the conformal mappings as long as the perturbation is small.

Asghar et al.[22] (1994) gives wind tunnel test results for a circular cone of semi-apex angle $\varepsilon = 8^\circ$ with a leeward fin of $h_L/a = 2.0$ at an angle of attack $\alpha = 35^\circ$ ($K = 4.9822$). The Reynolds number based on the base diameter D is $Re_D = 1.42 \times 10^5$. The separation angle is estimated to be $85^\circ < \theta_0 < 95^\circ$. The measured circumferential pressure distribution in a cross section and the distribution of the ratio of side force to normal force along the axis of the circular cone indicate that the flow becomes symmetric when the fin is added.

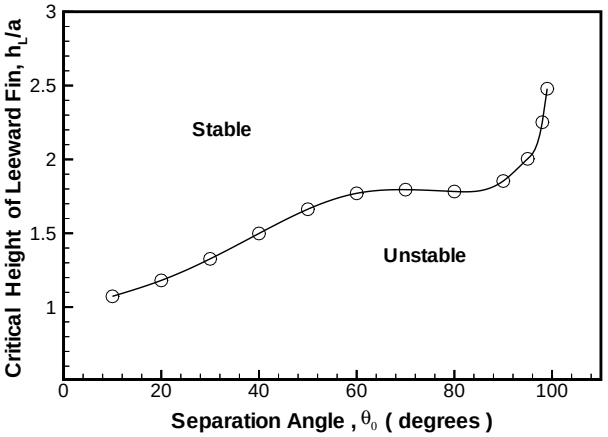

Fig. 9 Critical fin height vs. separation angle for a circular cone with fin, $K = 5.5591$**,** $h_W = 0.0$.

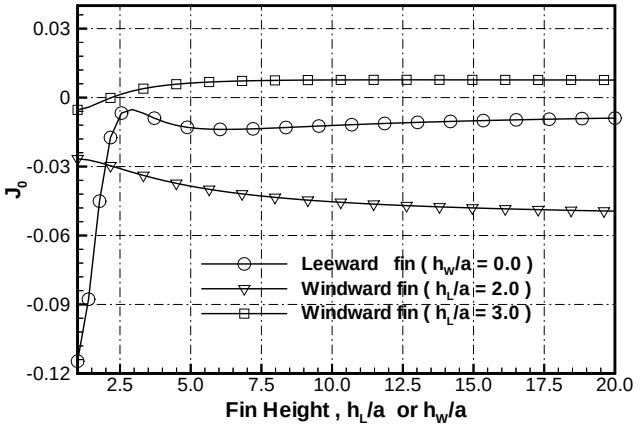

Fig. 10 Jacobian under anti-symmetric perturbations vs. leeward or windward fin height for a circular cone, $K = 5.5591, \theta_0 = 100^\circ$**.**

The present stability analyses are applied to this experimental case. Figs. 7 and 8 show the dependence of D_0 and J_0 on h_L/a with $K = 4.9822$ at $\theta_0 = 85^\circ$ and $\theta_0 = 95^\circ$, respectively. It is seen from Fig. 7 that for $\theta_0 = 85^\circ$, the vortex flow changes from unstable to stable at $h_L/a = 1.7828$, which is defined as the critical height of the fin. From Fig. 8, the critical height is 2.3833 for $\theta_0 = 95^\circ$. The present analytical result agree with the experimental results that a fin of $h_L/a = 2$ largely suppresses the vortex asymmetry that is present on the cone without the fin.

Fig. 9 shows the dependence of the critical height of the leeward fin on the circular cone on the separation angle θ_0 for $K = 5.5591$. At this value of K, the critical height of the leeward fin increases with θ_0 and increases rapidly when θ_0 approaches 100°.

An additional flat-plate triangular fin on the windward side is needed to suppress the vortex asymmetry when the separation point is at $\theta_0 \geq 100^\circ$ and $K = 5.5591$. Fig. 10 shows the variation of J_0 under anti-symmetric perturbations versus the fin heights h_L/a or h_W/a for $\theta_0 = 100^\circ$ and $K = 5.5591$. The corresponding divergence D_0 is given by Eq. (28) and is always negative. The Jacobian under symmetric perturbation is always positive. The line with circles in Fig. 10 shows J_0 versus the leeward fin size h_L/a when a windward fin is not used ($h_W/a = 0$). Although a leeward fin with $h_L/a > 2.5$ greatly improves the stability of the vortices, a leeward fin alone cannot suppress vortex asymmetry no matter its size. The line with triangles shows J_0 versus h_W/a when the leeward fin is fixed with $h_L/a = 2.0$. Adding a windward fin does not improve the stability of the vortices in this case. With a larger leeward fin $h_L/a = 3.0$ as shown by the line with squares in Fig. 10, however, addition of a windward fin of the size $h_W/a \geq 2.2022$ makes the initial unstable vortices stable. Further calculations indicate that if $h_L/a \geq 2.6295$, there exits a windward fin of finite height to suppress the vortex asymmetry, otherwise no such windward fin exists. Similarly, if $h_W/a \geq 2.1852$, there exists a leeward fin of finite height to suppress the vortex asymmetry, otherwise no such leeward fin exists. If an equal height is required for the leeward and windward fin to suppress the vortex asymmetry, $h_L/a = h_W/a \geq 2.7259$.

C. Slender Flat-Plate Delta Wing

The stability of the stationary vortex pair over the slender flat-plate delta wing was studied by Huang et al.[18] (1996) using the same simplified vortex model but a different method of stability analysis. They gave the stationary symmetric vortex position and strength versus K for $0.2 \leq K \leq 2.0$, and showed that the vortex flow is stable under small perturbations in the region $0.2 \leq K \leq 2.0$. The present stability theory is conveniently applied to study this problem and we extend the range of K investigated by Huang et al.[18] (1996). Fig. 11 gives the stationary vortex position and strength versus the similarity parameter K in the range of 0 to 10 for the slender flat-plate wing. The curves exactly overlap with the solutions by Huang, et.al[18] (1996) in the range of K calculated by them.

Fig. 12 shows that the symmetric vortex pair is stable under small symmetric and anti-symmetric perturbations for the entire range $0 < K \leq 10$. It can be seen that the degree of stability decreases monotonically as K increases and neutral stability is approached as K becomes large. Stahl[24] (1993) carried out flow-visualization experiments in a water tunnel. The Reynolds number based on the length of the model is $Re_L = 2.8 \times 10^4$. The delta wing model has sharp edges, a semi-apex angle $\varepsilon = 8^\circ$, and angle of attack $\alpha = 38^\circ$ (i.e. $K = 5.5591$). The experiments show that the leading-edge separation vortices over the wing remain symmetric before vortex break down occurs on the wing. This agrees with the predictions by Fig. 12.

Smith et al.[17] (1975) show that the two-dimensional

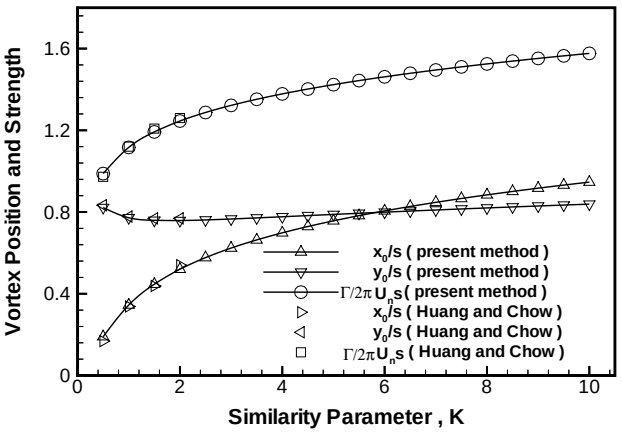

Fig. 11 Stationary vortex position and strength vs. similarity parameter for a triangular flat-plate wing, comparison with Huang and Chow (1996).[18]

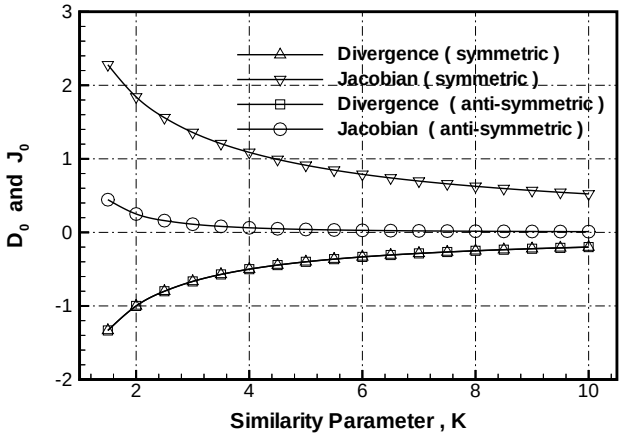

Fig. 12 Divergence and Jacobian vs. similarity parameter for a triangular flat-plate wing.

inviscid incompressible flow around a flat-plate normal to the freestream velocity has no stationary symmetric vortices behind the plate. In the corresponding three-dimensional case, however, such stationary symmetric vortices do exist over the slender flat-plate delta wing. The mechanism for the existence of such vortices in the three-dimensional case is the velocity $\mathbf{U}_c$ in Eqn. (13) induced by the axial component of the freestream velocity at the vortex, which tends to pull the vortex pair towards the center line of the flat-plate delta wing.

Under anti-symmetric perturbations, the symmetric vortex pair is unstable for the slender circular cone and is stable for the slender flat-plate wing. The reasons for this difference are the thickness effects of the circular cone in both the $\mathbf{U}_1$ and $\mathbf{U}_2$ parts of the solution discussed in Section 4. The instability effect due to thickness of the circular cone in the normal flow part is similar to that for the circular cylinder in the freestream flow which is to push the vortices away from the body. In addition, thickness of the circular cone also causes an effective expansion of the flow by a source term given in Eq. (18). In light of this, flow suction at the surface of the circular cone might be used to help stabilize the symmetric vortex pair at high angles of attack.

D. Slender Flat-Plate Delta Wing with Fin

Shanks[8] (1963) in his subsonic flow measurements found that the leading edge symmetric vortices over the flat-plate delta wing with $\varepsilon = 6°$ and a centerline spline of the height $h/s = 0.5$ became asymmetric at $\alpha \geq 24°$. This contradicts the observations by Stahl et al.[6] (1992). Ericsson[3] (1992) claimed that the vortex asymmetry was not due to hydrodynamic instability but rather likely due to asymmetric reattachment in the presence of the centerline spline on the leeside of the Shanks' wing model. This controversy leads to the following study of the vortex stability over the delta wing with a triangular flat plate fin in the leeside of the wing.

The contour of the slender flat-plane delta wing with a fin of the height h in the cross flow plane is mapped conformally into a circle by the three consecutive transformations.

$$Z = \frac{1}{2}\left(\rho - \frac{s^2}{\rho}\right) \tag{36}$$

$$\zeta' = \frac{1}{2}\left(\rho + \frac{s^2}{\rho}\right) \tag{37}$$

$$\zeta' - \xi_m = \frac{1}{2}\left(\zeta + \frac{{s_1}^2}{\zeta}\right) \tag{38}$$

where

$$\xi_m = \frac{(s-h_1)^2}{4h_1} \tag{39}$$

$$s_1 = \frac{(s+h_1)^2}{4h_1} \tag{40}$$

$$h_1 = h + \sqrt{h^2+s^2} \tag{41}$$

where s_1 is the radius of the circle in the plane ζ. The freestream flow velocity U_n in the plane Z is transformed into $U_n/2$ in the plane ζ. The complex velocity at the vortex Z_1 in the plane Z is given by Eq. (29) with U_n replaced by $U_n/2$, a replaced by s and a_1 replaced by s_1. The last term in Eq. (29) must be removed and $\frac{d\zeta}{dZ}$ and $\frac{d^2Z}{d\zeta^2}$ are given below

$$\frac{d\zeta}{dZ} = \frac{2\zeta^2(\rho^2-s^2)}{(\zeta^2-s_1^2)(\rho^2+s^2)} \tag{42}$$

$$\frac{d^2Z}{d\zeta^2} = \frac{s_1^2(\rho^2+s^2)}{(\rho^2-s^2)\zeta^3} - \frac{2s^2\rho^3(\zeta^2-s_1^2)^2}{\zeta^4(\rho^2-s^2)^3} \tag{43}$$

The divergence D_0 and the Jacobian J_0 at the stationary vortex position Z_0 under symmetric and anti-symmetric perturbations are evaluated from the complex velocity expression, and shown in Fig. 13 as

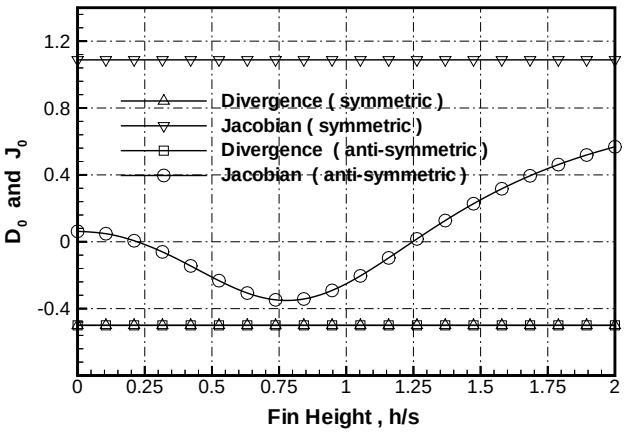

Fig. 13 Divergence and Jacobian vs. fin height for a triangular flat-plate wing with fin, $K = 4.0$.

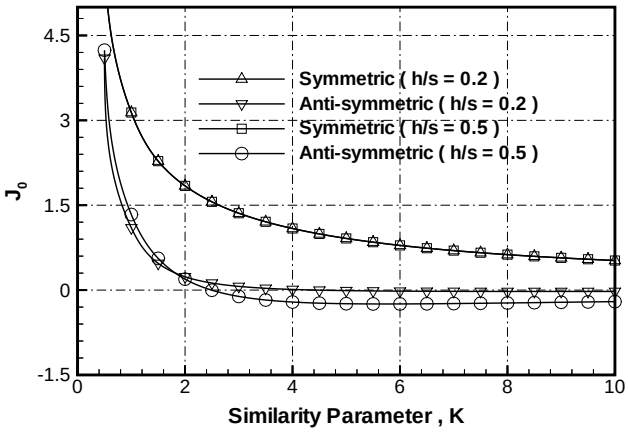

Fig. 14 Jacobian vs. similarity parameter for a triangular flat-plate wing with fin, $h/s = 0.2$ and $h/s = 0.5$.

a function of the fin height h/s for $K = 4.0$. It is seen that D_0 and J_0 are constants under symmetric perturbations as they should be. Under anti-symmetric perturbations, J_0 begins with positive value but decreases to zero as h/s increases to 0.2216. It then becomes negative and remains negative until $h/s = 1.2474$. Thus, according to our stability theory, adding a small lee-side fin in the range of $0.2216 < h/s < 1.2474$ causes the initially stable vortices over the delta wing to become unstable. Only when $h/s > 1.3059$ will the fin start to enhance the stability of the vortices compared to without the fin.

The front part of the Shanks' wing model, from the apex as far back as $x = c_0/2$ (c_0 is the root chord of the wing), resembles a flat-plate delta wing with a flat-plate triangular fin of the height $h/s \approx 0.5$. In the rear part $1/2 \leq x/c_0 \leq 1$ of the model, the centerline spline has a constant height equal to that at $x = c_0/2$. In order to compare with Shank's experimental setup, two cases are studied: (1) $h/s = 0.2$ and (2) $h/s = 0.5$. Fig. 14 shows the Jacobian J_0 versus the similarity parameter K under symmetric and anti-symmetric perturbations. When $h/s = 0.2$, the onset of the vortex flow asymmetry is at $K = 4.4414$, and when $h/s = 0.5$, the onset is at $K = 2.4929$. The experimental onset for the Shanks' model is at $K = 4.2361$. These results strongly suggest that the vortex asymmetry over the delta wing by Shanks and most likely other slender conical bodies is due to hydrodynamic instability.

E. Slender Elliptic Cone

The flat-plate delta wing and the circular cone can be seen as the limiting cases of an elliptic cone of thickness ratio τ (half-thickness/semi-span) as τ approaches 0 and 1, respectively. It is interesting to investigate how the stability property of the symmetric vortex flow over the slender elliptic cone changes from unstable to stable as the thickness ratio decreases from 1 to 0.

The conformal mapping for the ellipse in the plane Z to the circle of unit radius in a uniform flow of velocity $U_n/2$ in the plane ζ is

$$Z = \frac{1}{2}\left(\zeta + \frac{\lambda}{\zeta}\right) \tag{44}$$

where $c = \frac{1+\lambda}{2}$ and $b = \frac{1-\lambda}{2}$ are the semi-axes of the ellipse along the x and y axes, and $\tau = c/b$. Thus,

$$\frac{d\zeta}{dZ} = \frac{2\zeta^2}{\zeta^2 - \lambda} \tag{45}$$

$$\frac{d^2Z}{d\zeta^2} = \frac{\lambda}{\zeta^3} \tag{46}$$

To determine the stationary symmetric vortex position Z_0 and the vortex strength Γ, the tangential velocity on the elliptic contour is computed from the complex velocity expression

$$\begin{aligned} u - iv &= \left[\frac{U_n}{2}(1 - 1/\zeta^2) + \frac{i\Gamma}{2\pi}\left(\frac{1}{\zeta - \zeta_0}\right.\right. \\ &- \left.\left.\frac{1}{\zeta - \overline{\zeta_0}} - \frac{1}{\zeta - 1/\overline{\zeta_0}} + \frac{1}{\zeta - 1/\zeta_0}\right)\right]\left(\frac{d\zeta}{dZ}\right) \\ &- \frac{U_n\overline{Z}}{bK} + \frac{1}{2\pi}\sum_{j=1}^{n}\frac{Q_j}{Z - Z_j} \end{aligned} \tag{47}$$

To study the vortex stability the complex velocity at the vortex Z_1 is given by

$$\begin{aligned} u - iv &= \left[\frac{U_n}{2}(1 - 1/\zeta_1^2) + \frac{i\Gamma}{2\pi}\left(-\frac{1}{\zeta_1 - \zeta_2}\right.\right. \\ &- \left.\left.\frac{1}{\zeta_1 - 1/\overline{\zeta_1}} + \frac{1}{\zeta_1 - 1/\overline{\zeta_2}}\right)\right]\left(\frac{d\zeta}{dZ}\right)_1 \\ &- \frac{i\Gamma}{4\pi}\left(\frac{d^2Z}{d\zeta^2}\right)_1\left(\frac{d\zeta}{dZ}\right)_1^2 \\ &- \frac{U_n\overline{Z_1}}{bK} + \frac{1}{2\pi}\sum_{j=1}^{n}\frac{Q_j}{Z_1 - Z_j} \end{aligned} \tag{48}$$

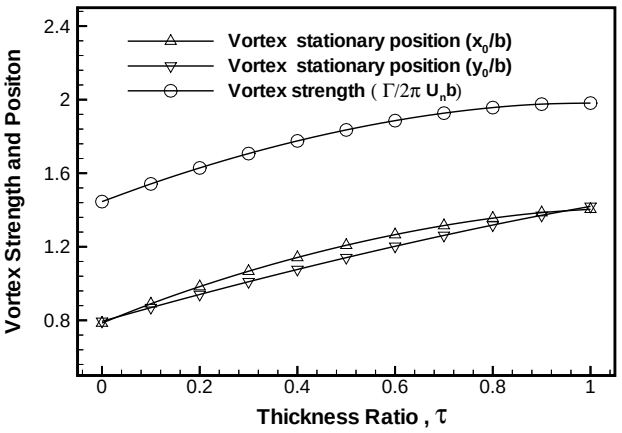

Fig. 15 Stationary vortex position and strength vs. thickness ratio for an elliptic cone, $K = 5.5591$, $\theta_0 = 90°$.

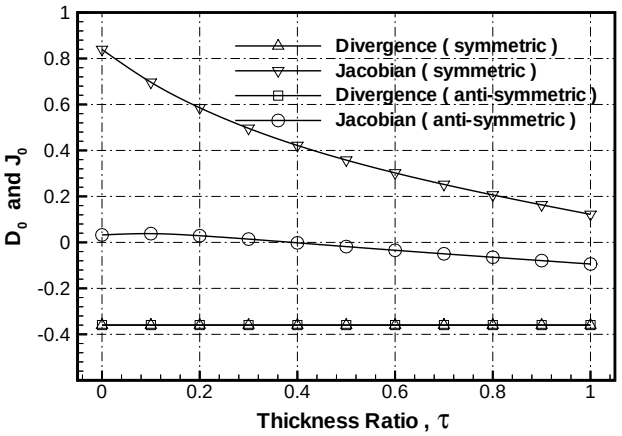

Fig. 16 Divergence and Jacobian vs. thickness ratio for an elliptic cone, $K = 5.5591$, $\theta_0 = 90°$.

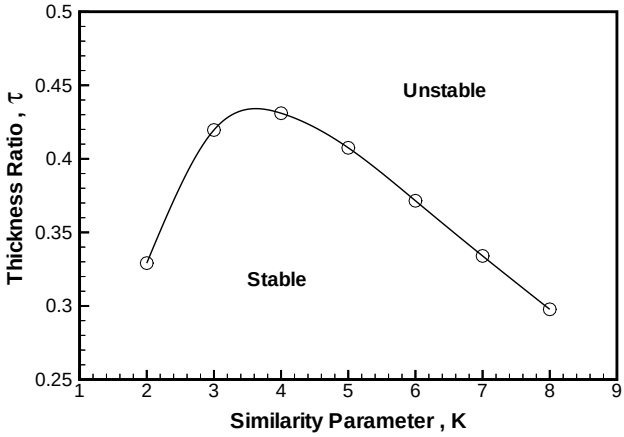

Fig. 17 Critical thickness ratio vs. similarity parameter for an elliptic cone, $\theta_0 = 90°$.

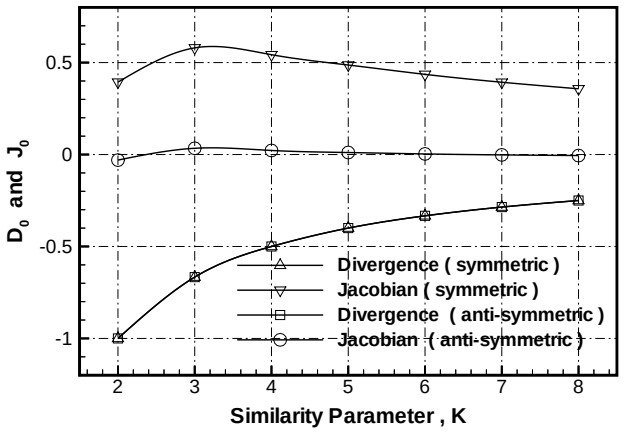

Fig. 18 Divergence and Jacobian vs. similarity parameter for an elliptic cone, $\tau = 0.35$, $\theta_0 = 90°$.

Stahl[24] (1993) presented the top and side views of the vortex configurations on the leeside of the delta wing and the elliptic cones with the thickness ratio $\tau = 0.40$, 0.65, and 1.0, for $\varepsilon = 8°$ at an angle of attack $\alpha = 38°$ (i.e., $K = 5.5591$). The main results showed that the degree of asymmetry of the vortex flow behind the elliptic cones decreases as the cone becomes flatter.

To compare with the experimental observation, Fig. 15 gives the stationary vortex position and strength and Fig. 16 plots D_0 and J_0 versus τ for the slender elliptic cone for $K = 5.5591$ and $\theta_0 = 90°$. The vortices change from being unstable to stable as τ decreases from 1 to 0. The critical thickness ratio for this transition is at $\tau = 0.389$. The agreement with Stahl's experimental observations is good on consideration that the separation position θ_0 was not given for the experiments by Stahl[24] (1993).

Fig. 17 shows the critical thickness ratio for the slender elliptic cone versus K for $\theta_0 = 90°$. The critical thickness of the elliptic cone has the maximum value $\tau = 0.4341$ at $K = 3.618$. Using vortex sheet and vortex line models, Fiddes et al.[13] (1989) compute numerically the vortex flow over slender elliptic cones and find that the vortices become essentially symmetric as the thickness ratio τ is decreased from 1 to 0.52 for the postulated separation position located at the leading edge, i.e., $\theta_0 = 90°$ and $\alpha/\varepsilon = 4.0$. From Fig. 17 the critical thickness ratio τ at $K = 4.0$ is 0.431, which is lower than 0.52 predicted by Fiddes et al.[13] (1989). It is noted that $\alpha/\varepsilon = 4.0$ given by Fiddes et al.[13] (1989) is approximately equivalent to $K = 4.0$ when ε is small.

Fig. 17 shows that the critical thickness ratio increases with increasing K until K reaches 3.618 for $\theta_0 = 90°$. This appears to be counter intuitive. Fig. 18 shows the Divergence D_0 and Jacobian J_0 for the slender elliptic cone with the thickness ratio $\tau = 0.35$ and $\theta_0 = 90°$. It is seen that the symmetric vortices remain stable in the finite interval of $2.3689 \leq K \leq 6.5574$.

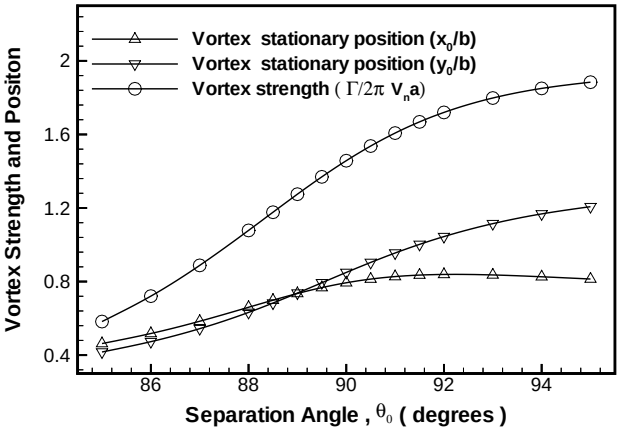

Fig. 19 Stationary vortex position and vortex strength vs. separation angle for an elliptic cone, $\tau = 0.10$, $K = 4.0$.

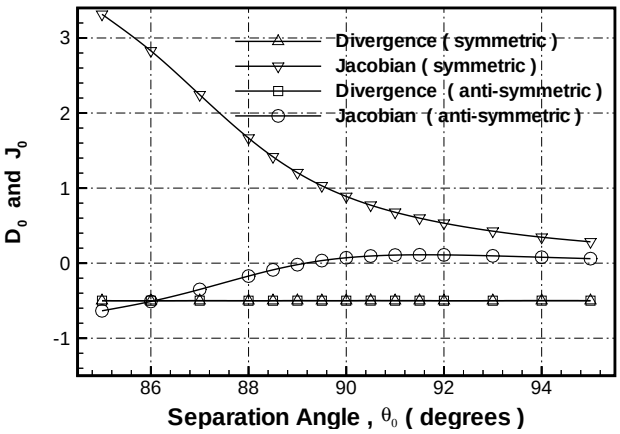

Fig. 20 Divergence and Jacobian vs. separation angle for an elliptic cone, $\tau = 0.10$, $K = 4.0$.

There is no available experimental data to verify this result.

Using tuft-grid surveys at low speeds, Bird[4] (1969) observed that the asymmetric vortex flow over a slender flat-plate delta wing model with a rounded leading edge and a semi-apex angle $\varepsilon = 3.5°$ occurs at $\alpha \geq 15°$, which disagrees with the observations by Stahl et al.[6] (1992), who used wing models with sharp leading edges. To investigate this controversy, a slender elliptic cone of thickness ratio $\tau = 0.1$ is considered for $K = 4.0$. The separation point may vary slightly around the round leading edge of the elliptic cone wing. Fig. 19 plots the stationary vortex position and vortex strength vs. the separation angle θ_0. Fig. 20 plots the divergence D_0 and Jacobian J_0 vs. the separation angle θ_0. The vortices are stable when the separation is exactly at the leading edge of the wing ($\theta_0 = 90°$). When the separation point moves from the leading edge to the windward side the symmetric vortex pair remains stable, but when the separation point moves

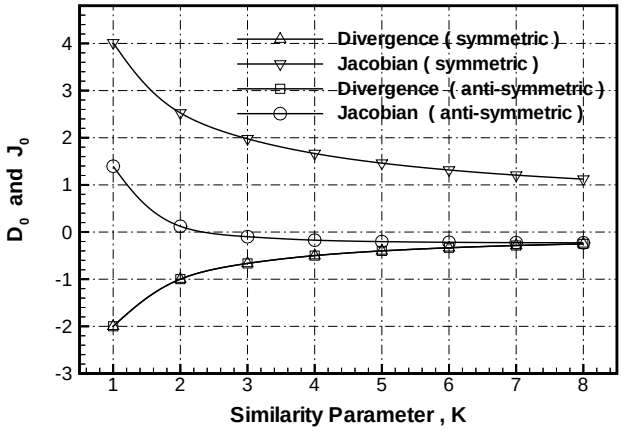

Fig. 21 Divergence and Jacobian vs. similarity parameter for an elliptic cone, $\tau = 0.10$, $\theta_0 = 88°$.

to the leeward side of the leading edge the vortices become less stable. They become neutrally stable at $\theta_0 = 89.17°$ and unstable when $\theta_0 < 89.17°$. The coordinates of this critical separation point ($\theta_0 = 89.17°$) are $x/b = 0.014337$ and $y/b = 0.989668$. They are very close to the coordinates of the leading edge at $x/b = 0.0$ and $y/b = 1.0$. Bird[4] (1969) did not provide details of his wing profile nor measurement of separation angles. If his wing model were to be represented by our elliptic cone with $\tau = 0.1$, the critical separation angle would be $\theta_0 = 89.3°$ with $K = 4.0$ and $\varepsilon = 3.5°$ given by his experiment. The asymmetry observed by Bird[4] (1969) may be due to such slight changes in the separation position on the round leading edge of his experimental models. This agrees with the experimental results of Lim et al.[7] (2001) on flat-plate wing of ogive-shaped planform with sharp/rounded tip and edges. For lack of experimental data on the separation position, no further quantitative comparison of the present analyses with Bird's experimental results is made here. It is clear, however, that the symmetry configuration of the leading-edge separated vortex flow over a highly swept delta wing can be controlled by slightly changing the separation position around the leading edge.

Fig. 21 shows D_0 and J_0 versus K for the elliptic cone with $\tau = 0.1$ and $\theta_0 = 88°$. The coordinates of this separation point ($\theta_0 = 88°$) are $x/b = 0.03297$ and $y/b = 0.94409$. The symmetric vortices over a delta wing with this elliptic profile become unstable at $K = 2.3658$.

To appreciate the physical meaning of the stability conditions in terms of D_0 and J_0, Fig. 22 and 23 show the vortex velocity field under anti-symmetric perturbations for the separation positions $\theta_0 = 90°$ and $85°$, respectively. The velocity vectors in Fig. 22 is drawn into the stationary point while circling around it. This is because the divergence D_0 is negative at the stationary point and the positive J_0 makes the eigenvalue for

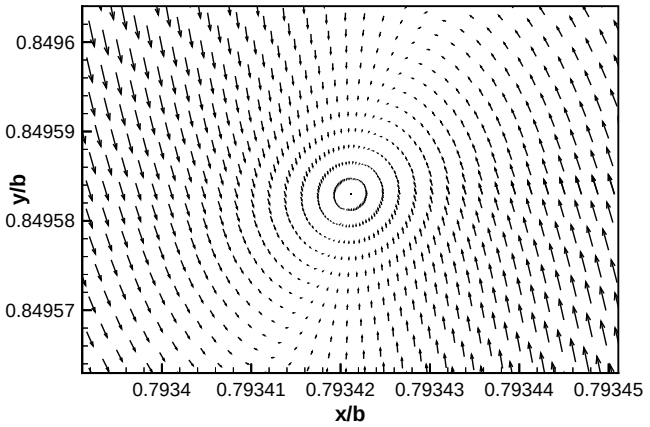

Fig. 22 Velocity of vortex under anti-symmetric perturbations for the flow over an elliptic cone, $\tau = 0.1$, $K = 4.0$, $\theta_0 = 90^\circ$ (stable case).

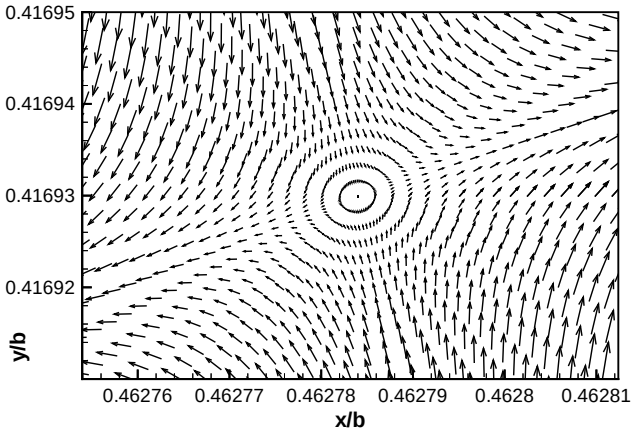

Fig. 23 Velocity of vortex under anti-symmetric perturbations for the flow over an elliptic cone, $\tau = 0.1$, $K = 4.0$, $\theta_0 = 85^\circ$ (unstable case).

the motion of the vortex contain an imaginary part that gives rise to the oscillatory motion (see Cai et al.[19] 2001).

Fig. 23 shows an unstable case when $J_0 < 0$. Although D_0 is still negative in this case, a negative J_0 renders at least some velocity vectors to leave the stationary point, which leads to possible runaway of the vortex when slightly perturbed from its stationary location.

VII. Conclusions

The onset of asymmetry of initially symmetric vortex flow over slender conical bodies at high angles of attack at low speed is identified as a result of vortex stability under small anti-symmetric perturbations by a simplified line vortex inviscid model with postulated symmetric separation positions and using a new stability condition by the authors. Problems of slender circular cones and highly swept delta wings with and without fins, and slender elliptic cones of various eccentricities are studied. The following conclusions are drawn.

1. Stationary symmetric vortices exist over circular cones and are stable under small symmetric perturbations, but unstable under small anti-symmetric perturbations.

2. For highly swept flat-plate delta wing, the vortex flow over the wing is stable under small perturbations and thus remains symmetric before vortex breakdown occurs on the wing.

3. For slender elliptic cones of various thickness ratios (half-thickness /semi-span) at high angles of attack, the degree of the vortex asymmetry decreases monotonically as the thickness ratio decreases from 1 to 0.

4. The vortex asymmetry over a slender circular cone can be suppressed by adding a flat-plate triangular fin of sufficient height in the incidence plane of the cone. When the separation lines are located on the leeside of the cone, a fin on the leeward side is sufficient. When the separation lines are on the windward side of the cone, fins on both leeward and windward sides are needed to suppress the vortex asymmetry.

5. A fin of very low height added to a slender circular cone or a flat-plate triangular wing, however, has the opposite effect, i.e., it destabilizes the vortex flow.

6. Vortices over highly swept thin delta wings with round leading edges are sensitive to slight changes of the separation position around the leading edge. A slight shift from the leading edge to a nearby point on the leeside of the wing may lead to the onset of vortex asymmetry at some high angle of attack.

7. It is the effect of the axial velocity component on the vortex line which pulls the vortex line towards the body axis ($\mathbf{U}_c$ in Eqn. (13)) that helps to trap and stabilize the symmetric vortex pair over a three-dimensional body at high angles of attack. Due to the lack of this effect, a symmetric vortex pair in a two-dimensional flow can never be stable.

8. Body thickness in the incidence plane pushes the vortex line away from the body axis and decreases the stability of the symmetric vortex pair.

9. For all the three-dimensional bodies studied, the symmetric vortex pair over the body is stable under small symmetric perturbations, and may be unstable, neutrally stable, or stable under anti-symmetric perturbations depending on the thickness ratio, the separation position and the Sychev

similarity parameter. In general the vortices become less stable with increasing thickness ratio, more stable as the flow separation moves towards the windward side of the body, and less stable with increasing Sychev parameter.

10. For all the slender conical bodies studied, the distance between the separation vortex and the body axis has the same order of magnitude as the body lateral dimension for all possible separation positions and K as high as 10. This verifies the validity of the assumption that the body and its separation vortices as a whole is slender in the current model.

11. Agreement with known experimental observations indicate that the analysis presented in this paper is able to predict qualitative features of the high angle of attack flow around slender conical bodies. The presented stability analysis strongly supports the belief that the occurrence of vortex asymmetry over slender bodies at high angles of attach is due to hydrodynamic instability.

References

[1]Ericsson, L. and Reding, J., "Asymmetric flow separation and vortex shedding on bodies of revolution," *Tactical Missile Aerodynamics: General Topics*, 1992, pp. 391–452, 2nd ed,. edited by M.J. Hemsch, Progress in Astronautics and Aeronautics.

[2]Keener, E., "Similarity in vortex asymmetries over slender bodies and wings," *AIAA Journal*, Vol. 15, 1977, pp. 1370–1372.

[3]Ericsson, L., "Sources of high alpha vortex asymmetry at zero sideslip," *Journal of Aircraft*, Vol. 29, 1992, pp. 1086–1090.

[4]Bird, J., "Tuft-grid surveys at low speeds for delta wing," NASA TN D-5045, 1969.

[5]Polhamus, E., "Predictions of vortex-lift characteristics by a leading-edge suction analogy," *Journal of Aircraft*, Vol. 8, 1971, pp. 193–199.

[6]Stahl, W., Mahmood, M., and Asghar, A., "Experimental investigations of the vortex flow on delta wings at high incidence," *AIAA Journal*, Vol. 30, 1992, pp. 1027–1032.

[7]Lim, T., Lua, K., and Luo, S., "Role of tip and edge geometry on vortex asymmetry," *AIAA Journal*, Vol. 39, 2001, pp. 539–543.

[8]Shanks, R., "Low-subsonic measurements of static and dynamic stability derivatives of six flat-plate wing having leading-edge sweep angles of 70° to 84°," NASA TN D-1822, 1963.

[9]Stahl, W., "Suppression of vortex asymmetry behind circular cones," *AIAA Journal*, Vol. 28, 1990, pp. 1138–1140.

[10]Ng, T., "Effect of a single strake on the fore body vortex asymmetry," *Journal of Aircraft*, Vol. 27, 1990, pp. 844–846.

[11]Edwards, O., "Northrop F-5F shark nose development," NASA CR 158936, 1978.

[12]Dyer, D. E., Fiddees, S. P., and Smith, J. H. B., "Asymmetric vortex formation from cones at incidence – a simple inviscid model," *Aeronautical Quarterly*, Vol. 31, 1982, pp. 293–312.

[13]Fiddes, S. and Williams, A., "Recent developments in the study of separated flow past slender bodies at incidence," *Symposium on the Prediction and Exploitation of Separated Flow*, Royal Aeronautical Society, 1989, pp. 31.1–31.17.

[14]Lowson, M. and Ponton, A., "Symmetry breaking in vortex flows on conical bodies," *AIAA Journal*, Vol. 30, 1992, pp. 1576–1583.

[15]Fiddes, S., "A theory of the separated flow past a slender elliptic cone at incidence," AGARD Paper CP291 30, 1980, Computation of Viscous-Inviscid Interactions.

[16]Föppl, L., "Wirbelbewegung hinter einem Kreiszylinder," *Sitzb. d. k. baeyr, Akad. d. Wiss., Math-Physi. Klasse, Müchen*, Vol. 1, 1913, pp. 1–17.

[17]Smith, J. H. B. and Clark, R. W., "Non-existence of stationary vortices behind a two-dimensional normal plate," *AIAA Journal*, Vol. 13, 1975, pp. 1114–1115.

[18]Huang, M. K. and Chow, C. Y., "Stability of leading-edge vortex pair on a slender delta wing," *AIAA Journal*, Vol. 34, 1996, pp. 1182–1187.

[19]Cai, J., Liu, F., and Luo, S., "Stability of symmetric vortices behind two-dimensional bodies," AIAA Paper 2001-2844, June 2001.

[20]Sychev, V., "Three-dimensional hypersonic gas flow past slender bodies at high angle of attack," *Journal of Maths and Mech. (USSR)*, Vol. 24, 1960, pp. 296–306.

[21]Saffman, P., *Vortex Dynamics*, Cambridge University Press, Cambridge, 1992.

[22]Asghar, A., Stahl, W., and Mahmood, M., "Suppression of vortex asymmetry and side force on a circular cone," *AIAA Journal*, Vol. 32, 1994, pp. 2117–2120.

[23]Rossow, V. J., "Lift enhancement by an externally trapped vortex," *Journal of Aircraft*, Vol. 15, 1978, pp. 618–625.

[24]Stahl, W., "Experimental investigations of asymmetric vortex flows behind elliptic cones at incidence," *AIAA Journal*, Vol. 31, 1993, pp. 966–968.